

Check of Earth's free oscillations excited by Sumatra-Andaman Large Earthquake and discussions on the anisotropy of inner core

LEI XiangE^{1,2†}, SUN HePing¹, HSU HouTse¹ & SHI YaoLin²

¹ Key Laboratory of Dynamic Geodesy, Institute of Geodesy and Geophysics, Chinese Academy of Sciences, Wuhan 430077, China;

² Laboratory of Computational Geodynamics, Graduate University of Chinese Academy of Sciences, Beijing 100049, China

Sumatra-Andaman Large Earthquake on Dec. 26, 2004 generated not only the Indian Ocean Tsunami but also the Earth's free oscillations (EFO). The signals of Earth's free oscillations were perfectly recorded by the superconducting gravimeter C0-32 at Wuhan station in China. After the pre-treatment and spectral analysis on the observational data from Wuhan station, we obtained more than ninety EFO modes including 42 fundamental modes, 2 radial modes and 49 harmonic modes. On the basis of the discussions on some observed harmonic modes and abnormal splitting phenomena, we considered that the real rigidity might be lower than the theoretical prediction of PREM model in the inner core and however the anisotropy of compressive wave was brightly higher than the present estimations in the inner core. This suggested that the anisotropy of the inner core could be much more complicated than our present understanding, and there might be some new geophysical phenomena in the formation process of the inner core.

Sumatra-Andaman Large Earthquake, Earth's free oscillations, superconducting gravimeter, abnormal spectral splitting, anisotropy of inner core

There was Sumatra-Andaman Large Earthquake more than 9.0 M_w occurring in the Indian Ocean west of Sumatra Island on Dec. 26, 2004, which has been one of the largest earthquakes since 1964. The earthquake generated the Indian Ocean Tsunami roaring the coast of Southeast Asia, at the same time it still excited the Earth's free oscillations (EFO). The observation of EFO was not only helpful to determining accurately the amplitude of this huge earthquake, but also to providing a precious chance for us to study the deep structure of the Earth^[1,2].

The Earth's free oscillations consist of two basic series: toroidal modes and spheroidal modes containing the radial deformation of the Earth's surface. Superconducting gravimeters (SG) are one kind of very reliable and accurate instruments to investigate the vertical deformation of the Earth's surface and the variation of the Earth's gravity field, which can catch the Earth's gravity

field variation within the period range from seconds to years at very low noise level^[3]. So SG has an excellent capacity of checking the Earth's free oscillations. It is one of research contents of the Global Geodynamic Project (GGP) and also an international frontier in the correlative earth-science field that the EFO phenomena were checked with SG^[4,5].

The accident of Sumatra-Andaman Large Earthquake was accurately recorded by SG C0-32 at Wuhan station under Institute of Geodesy and Geophysics, Chinese Academy of Sciences. After the pre-treatment and spectral analysis for the observational data, we obtained a total of 93 EFO modes and the spectral splitting of 12

Received August 10, 2006; accepted October 13, 2006

doi: 10.1007/s11430-007-0028-6

†Corresponding author (email: leixe@asch.whigg.ac.cn)

Supported jointly by the National Natural Science Foundation of China (Grant Nos. 40404005 and 40374029) and the Excellent Prize of President Scholarship and Hundred Talents Program of the Chinese Academy of Sciences

EFO modes.

1 Observational data and pre-treatment

A more than 9.0 M_w huge earthquake (95.95°E, 3.31°N) occurred in the Indian Ocean west of Sumatra Island at 00:58:53 on Dec. 26, 2004 (UT). Stein and Okal^[1] pointed out that the earthquake could arrive at 9.3 M_w by analyzing the observational recording of seismographs. Park et al.^[2] considered that the amplitude of the earthquake is about 9.15 M_w by the comprehensive discussions on the observations from strainmeters, long-period seismographs and superconducting gravimeters. In general, the Sumatra-Andaman Earthquake has been one of the largest earthquakes in the globe since 1964. The superconducting gravimeter (SG) No.C0-32 was set up in the geodynamic observation station of the Jiufeng Mountain nearby Wuhan City in 1997, which belongs to Institute of Geodesy and Geophysics, Chinese Academy of Sciences. The observational data were recorded by the instrument depending on a set of highly accurate digital collection systems and with the sampling time signals provided by GPS clock. The sampling ratio is 10 seconds for both gravity values and the pressure values. The calibration of the SG C0-32 was realized by the same address observation of several absolute gravimeters (FG5). The calibration value of SG C0-32 is $-84.6550 \cdot 10^{-8} \text{M} \cdot \text{S}^{-2} / \text{mV}^{[6]}$. Because most of EFO modes usually last only several days, we can neglect the influence of some long-period term variations in the Earth's gravity field such as polar migration. For the check of the Earth's free oscillations, the pre-treatment of the SG data consists of the removal of gravity tides, the correction of pressure effect and the appraisal of observational background noise.

The removal of gravity tides can be theoretically realized by the computation of synthetic tides, but it needs several years of observation data to determine accurately the tidal parameters^[7-9]. So the former researchers^[10-12] usually removed the tidal signals from the observational data with digital filters instead of the calculation of synthetic tides. In view of possible abasement of some low-class mode and unsatisfied frequency-phase characteristics of some digital filters, we have adopted the method of fragmental polynomial fitting to remove the gravity tides^[13]. This process includes twice polynomial fittings, the first fitting is of 20-class polynomial and the second is of 10-class polynomial. The optimal passage

length is about a half day for the fragmental polynomial fitting, the gravity tides were removed fully from the observational SG data, at the same time, the low-class and high-class EFO modes were excellently kept in the observational residuals of SG data^[14].

The second step of pre-treatment was the correction of pressure effect. Although it is complex to directly consider the effect of atmosphere variation on the gravity observation at station, some scholars^[15-17] found that the correction of pressure effect could be simply expressed as the multiplication of the pressure variation ΔP and an atmospheric gravity admittance A , and their investigations showed that it could gain high accuracy to apply the atmospheric admittance to the correction of pressure effect. Sun^[18] gained the theoretical atmosphere admittance at Wuhan station ($A = -0.3603 \mu\text{Gal}/\text{hPa}$) by the computation of atmospheric gravity Green's function. Xu et al.^[19] got the experimental atmospheric admittance ($A = -0.307 \mu\text{Gal}/\text{hPa}$) by the analysis of the observation data of SG C0-32. Luo^[20] simulated the atmospheric gravity effect at Wuhan station with the global temperature and pressure data, and got an atmospheric admittance: $A = -0.336 \mu\text{Gal}/\text{hPa}$. We have adopted some different admittance values from $-0.3603 \mu\text{Gal}/\text{hPa}$ to $-0.307 \mu\text{Gal}/\text{hPa}$, there was only small discrepancy among these admittances. Our experiments showed that it was suitable to adopt the admittance value $A = -0.326 \mu\text{Gal}/\text{hPa}$ for the correction of pressure effect at Wuhan station. Zürn et al.^[21] and Van Camp^[11] considered that the background noise below 1.2 mHz could be effectively decreased by the correction of pressure effect; however, our results showed that it was only below 0.8 mHz that the check of EFO signals was clearly improved by the correction of pressure effect at Wuhan station. In fact, the EFO signals have already been the main element of the observational residuals after the removal of gravity tides and the correction of pressure effect, the amplitude of which showed a temporal decay with the exponential form^[14].

The SG observation noise is so complicated that we cannot have an analytic method to describe directly it during EFO^[11]. The SG observation noise mainly includes the observation noise of instrument itself and the local background noise around SG station. Banka^[22] introduced a method of the noise magnitude of earthquake (abbrev: Mn method) to estimate the observation noise of SG, in which Banka took the observational-

residuals spectrum in the frequency range of 1.67–9.9 mHz as a part of the observation noise spectrum of SG; however in fact, there were the abundant spectral peaks of EFO modes in this frequency range. For this reason, we introduced a new method to simulate the observation noise of SG with the observational residuals in the quiet earthquake period before and after a large earthquake. Sumatra-Andaman Large Earthquake was so huge that it was still not quiet after the earthquake, so we adopted the observational residuals in the quiet period before the earthquake as the simulation of the observation noise of SG C0-32. Applied Fast Fourier Transform (FFT) to the observational residuals, we gained the simulated noise spectrum (abbrev: SNS) of SG observation. Although SNS is not equal to the real noise spectrum of SG C0-32 during EFO, it is reasonable and effective to describe the real noise spectrum during EFO, because it is a case that the observation noise of SG itself is very stable and the local noise around station can have only a small change in a short time. In Figure 1(a), we show the simulated observation noise of SG C0-32. To provide a convenient evaluation for the reliability of observed EFO modes, we used the average value of SNS in a narrow frequency

range covering a mode to describe the noise level nearby this mode and it was marked as $NL_{MODE}^{[14]}$.

2 Spectrum analysis and check of Earth's free oscillation

The former scholars have applied three kinds of spectral analysis methods to catch the signals of the Earth's free oscillations, which included Fast Fourier Transform (FFT)^[10,11,13], wavelet analysis^[12] and maximum entropy spectrum^[1,23]. The maximum entropy spectrum can provide a very high frequency resolution, however it is only suitable for the continuous stable signals. The wavelet analysis has an excellent temporal resolution on the observational signal, while FFT can provide a good frequency resolution on the EFO signals. Because our focus was on the accurate check of EFO frequencies, we applied FFT to the observational residuals for checking EFO signals, which is also convenient for the estimation of Signal-to-Noise Ratio of observed EFO modes. In Figure 1(b), we show the spectral peaks of EFO modes excited by Sumatra-Andaman Large Earthquake. The checked EFO signal was a passage of observational residuals of about 112.2 hours, so the frequency-resolution ratio (FRR) of FFT was approximately equal to $2.6 \times 10^{-6} \text{ Hz}$ for EFO spectral peaks. The Signal-to-Noise Ratio (SNR) of an EFO mode was defined as a rate between the spectral peak value of a mode and the NL_{MODE} covering the mode. If SNR value of a checked EFO mode was more than 3.0, we considered it as the believable and adopted mode. In total, we have obtained 94 EFO modes including 42 fundamental modes, 2 radial modes and 49 harmonic modes.

We provide the observed 42 modes in Table 1, and the theoretical predictions of PREM model (<http://www-gpi.physik.uni-karlsruhe.de/pub/widmer/Modes/modes.html> MINOS Program) are also listed as a comparison. All basic modes were checked except ${}_0S_{33}$ and ${}_0S_{43}$ modes in the fundamental mode series from ${}_0S_0$ to ${}_0S_{44}$. Apart from ${}_0S_{26}$, ${}_0S_{35}$, ${}_0S_{41}$ and ${}_0S_{44}$ modes, the other checked basic modes had no more than a multiple of FRR discrepancy from the theoretical predictions. There were two reasons to explain why the four modes occupy the larger discrepancies from the theoretical predictions. The first possible explanation was that the four modes may have some nodal lines nearby Wuhan station, so their spectral peaks have small amplitudes and low SNR. The other reason may originate from a zone with

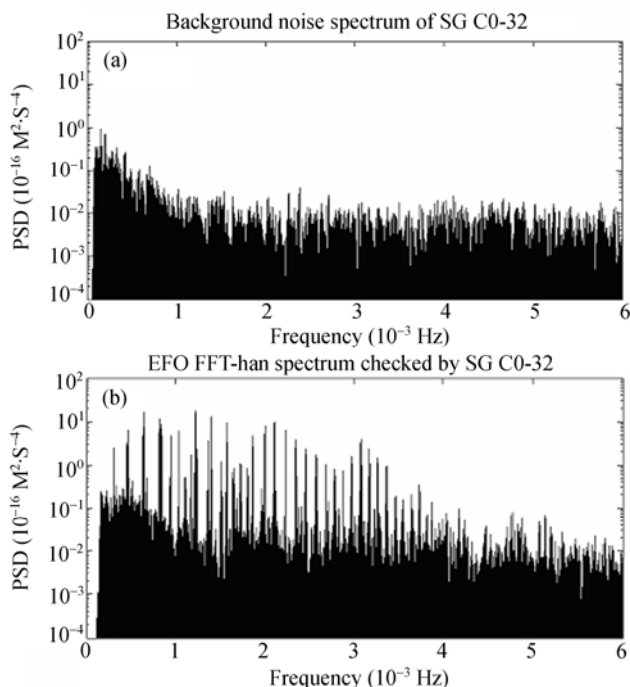


Figure 1 The simulated observation noise of SG C0-32. Horizontal ordinate is frequency, vertical ordinate is power spectral density. (a) The background noise spectrum of SG C0-32 at Wuhan station before Sumatra-Andaman Large Earthquake; (b) the power spectrum of EFO signals excited by Sumatra-Andaman Large Earthquake.

Table 1 Comparison between the checked 42 fundamental and the theoretical predictions of PREM model, as well as the checked 2 radial modes

Basic modes	${}_0S_0$	${}_0S_2$	${}_0S_3$	${}_0S_4$	${}_0S_5$	${}_0S_6$	${}_0S_7$	${}_0S_8$	${}_0S_9$	${}_0S_{10}$
Observation (10^{-3} Hz)	0.8145	0.3095	0.4687	0.6474	0.8393	1.0386	1.2304	1.4112	1.5770	1.7256
PREM (10^{-3} Hz)	0.8143	0.3093	0.4686	0.6471	0.8404	1.0382	1.2318	1.4135	1.5783	1.7265
Basic modes	${}_0S_{11}$	${}_0S_{12}$	${}_0S_{13}$	${}_0S_{14}$	${}_0S_{15}$	${}_0S_{16}$	${}_0S_{17}$	${}_0S_{18}$	${}_0S_{19}$	${}_0S_{20}$
Observation (10^{-3} Hz)	1.8642	1.9905	2.1143	2.2331	2.3470	2.4609	2.5698	2.6763	2.7778	2.8793
PREM (10^{-3} Hz)	1.8624	1.9904	2.1129	2.2314	2.3464	2.4582	2.5671	2.6733	2.7770	2.8784
Basic modes	${}_0S_{21}$	${}_0S_{22}$	${}_0S_{23}$	${}_0S_{24}$	${}_0S_{25}$	${}_0S_{26}$	${}_0S_{27}$	${}_0S_{28}$	${}_0S_{29}$	${}_0S_{30}$
Observation (10^{-3} Hz)	2.9783	3.0749	3.1714	3.2655	3.3621	3.4561	3.5453	3.6344	3.7235	3.8176
PREM (10^{-3} Hz)	2.9777	3.0753	3.1713	3.2659	3.3659	3.4519	3.5437	3.6348	3.7253	3.8155
Basic modes	${}_0S_{31}$	${}_0S_{32}$	${}_0S_{33}$	${}_0S_{34}$	${}_0S_{35}$	${}_0S_{36}$	${}_0S_{37}$	${}_0S_{38}$	${}_0S_{39}$	${}_0S_{40}$
Observation (10^{-3} Hz)	3.9067	3.9983		4.1716	4.2583	4.3548	4.4415	4.5281	4.6222	4.7113
PREM (10^{-3} Hz)	3.9054	3.9950		4.1739	4.2632	4.3525	4.4418	4.5312	4.6206	4.7101
Basic modes	${}_0S_{41}$	${}_0S_{42}$	${}_0S_{43}$	${}_0S_{44}$	Radial modes			${}_1S_0$	${}_4S_0$	
Observation (10^{-3} Hz)	4.7930	4.8896		5.0654	Observation (10^{-3} Hz)			1.6315	4.1097	
PREM (10^{-3} Hz)	4.7997	4.8893		5.0690	PREM (10^{-3} Hz)			1.6313	4.1058	

strong lateral heterogeneity in the upper mantle, which had an effect on the frequencies of these observed modes. We observed three radial modes including ${}_0S_0$, ${}_1S_0$ and ${}_4S_0$. Among them, the ${}_0S_0$ mode could be looked on as a fundamental mode too, and the ${}_1S_0$ and ${}_4S_0$ modes are listed after ${}_0S_{44}$ mode in Table 1. The SNR of ${}_1S_0$ and ${}_4S_0$ mode separately reached 33.0 and 5.0, so the ${}_1S_0$ mode agreed with the PREM model better than ${}_4S_0$ mode, yet the discrepancy of ${}_4S_0$ mode was still no more than 2 multiples of FRR.

In general, shallow-focus earthquakes mainly generate fundamental EFO modes, however Sumatra-Andaman Large Earthquake was so huge that it excited not only fundamental EFO modes but also abundant harmonic modes. We observed a total of 49 harmonic modes excited by Sumatra-Andaman Large Earthquake. The checked harmonic modes are provided in Table 2, as the reference, we listed the theoretical predictions of PREM model^[24] provided by MINOS Program. The excitation of EFO modes presented an unbalanced distribution in different degrees, Sumatra-Andaman Large Earthquake fully excited the 1-degree (9 modes), 5-degree (8 modes) and 7-degree (7 modes) harmonic modes. Among the checked harmonic modes, six modes (including ${}_5S_7$, ${}_5S_{14}$, ${}_9S_4$, ${}_7S_{10}$, ${}_7S_{13}$ and ${}_{12}S_1$) had 1.7 multiples of FRR about 4.0×10^{-6} Hz discrepancy from the theoretical predictions of PREM model, especially ${}_7S_{10}$, ${}_7S_{13}$ and ${}_{12}S_1$ modes separately occupied the discrepancies of -9.4×10^{-6} Hz, -7.4×10^{-6} Hz and 7.5×10^{-6} Hz according to about 3 multiples of FRR from PREM model. It showed that the checked modes were reliable that the three modes respectively occupied the SNR values of 13.2, 5.0 and 5.7.

On the basis of the displacement field of EFO modes, Prof. Gilbert and Prof. Masters at the University of California, San Diego calculated the distributions of elastic-wave energy density of EFO modes (<http://www-gpi.physik.uni-karlsruhe.de/pub/widmer/Modes/modes.html> MINOS Program) within the Earth, which consisted of compressive-energy and shear-energy density distribution for spheroidal modes. This kind of elastic-wave energy distribution was usually called the kernel functions of EFO modes, because they directly mirrored the sensitivity of EFO modes to the elastic parameters of media in the different depth in the Earth. The kernel functions of some modes (including ${}_0S_{24}$, ${}_{12}S_1$, ${}_1S_4$, ${}_0S_3$, ${}_8S_6$, ${}_{10}S_2$, ${}_{13}S_2$ and ${}_7S_{13}$) were provided by MINOS Program and are presented in Figure 2. The elastic-energy density of ${}_0S_{24}$ mode is higher in the upper mantle and the crust than in other layers, therefore ${}_0S_{24}$ mode is sensitive to the elastic parameters in the upper mantle and the crust, and this kind of EFO modes is called ‘surface-wave equivalent’ modes. As the similar reason, ${}_{12}S_1$, ${}_1S_4$ and ${}_0S_3$ modes are sensitive to the shear-wave parameters in the mantle, and they is usually called ‘mantles-equivalent’ modes. The propagation of ${}_8S_6$ mode has reached the outer core, so it is often called ‘PKP-equivalent’ mode, and ${}_7S_{10}$ is a similar mode. ${}_{10}S_2$ and ${}_{13}S_2$ modes are usually called ‘PKIKP-equivalent’ modes, because their propagations have arrived at the inner core. The shear-energy density of ${}_{10}S_2$ mode is high in the top of the inner core as well as the compressive-energy density of ${}_{13}S_2$ mode. The role that the anisotropy of the inner core played in the spectral splitting of ${}_{10}S_2$ and ${}_{13}S_2$ modes was more important, compared with the effect of the anisotropy of the outer core and the

Table 2 Comparison between the checked 50 harmonic modes and the theoretical predictions of PREM model

1-degree	${}_1S_2$	${}_1S_4$	${}_1S_6$	${}_1S_7$	${}_1S_8$	${}_1S_9$	${}_1S_{18}$	${}_1S_{22}$	${}_1S_{29}$
Observation (10^{-3} Hz)	0.6808	1.1747	1.5251	1.6538	1.8023	1.9657	3.6418	4.2310	5.2387
PREM (10^{-3} Hz)	0.6799	1.1729	1.5220	1.6555	1.7993	1.9637	3.6449	4.2344	5.2393
2-degree	${}_2S_3$	${}_2S_4$	${}_2S_5$	${}_2S_6$	${}_2S_{16}$				
Observation (10^{-3} Hz)	1.2453	1.3765	1.5127	1.6835	3.4438				
PREM (10^{-3} Hz)	1.2422	1.3792	1.5149	1.6808	3.4435				
3-degree	${}_3S_1$	${}_3S_2$	${}_3S_8$	${}_3S_{15}$	${}_3S_{21}$				
Observation (10^{-3} Hz)	0.9457	1.1029	2.8199	3.8126	4.7732				
PREM (10^{-3} Hz)	0.9440	1.1062	2.8196	3.8105	4.7726				
4-degree	${}_4S_2$	${}_4S_9$	${}_4S_{19}$						
Observation (10^{-3} Hz)	1.7206	3.7087	5.2065						
PREM (10^{-3} Hz)	1.7223	3.7087	5.2065						
5-degree	${}_5S_4$	${}_5S_5$	${}_5S_7$	${}_5S_8$	${}_5S_{11}$	${}_5S_{13}$	${}_5S_{14}$	${}_5S_{15}$	
Observation (10^{-3} Hz)	2.3780	2.7035	3.2952	3.5279	4.4588	4.9218	5.1322	5.3303	
PREM (10^{-3} Hz)	2.3795	2.7034	3.2908	3.5257	4.4566	4.9244	5.1368	5.3301	
6-degree	${}_6S_3$	${}_6S_7$							
Observation (10^{-3} Hz)	2.8248	3.5502							
PREM (10^{-3} Hz)	2.8217	3.5526							
7-degree	${}_7S_5$	${}_7S_6$	${}_7S_7$	${}_7S_8$	${}_7S_{10}$	${}_7S_{11}$	${}_7S_{13}$		
Observation (10^{-3} Hz)	3.6616	3.9612	4.2360	4.4489	4.7584	4.9143	5.2808		
PREM (10^{-3} Hz)	3.6598	3.9587	4.2379	4.4526	4.7678	4.9169	5.2882		
8-degree	${}_8S_1$	${}_8S_5$	${}_8S_6$						
Observation (10^{-3} Hz)	2.8719	4.1667	4.4316						
PREM (10^{-3} Hz)	2.8734	4.1662	4.4352						
9-degree	${}_9S_2$	${}_9S_4$	${}_9S_7$						
Observation (10^{-3} Hz)	3.2284	3.8721	4.8673						
PREM (10^{-3} Hz)	3.2318	3.8780	4.8726						
More than 10-degree	${}_{10}S_2$	${}_{10}S_5$	${}_{11}S_5$	${}_{12}S_1$	${}_{13}S_2$	${}_{13}S_3$			
Observation (10^{-3} Hz)	4.0355	4.4687	5.0728	4.3078	4.8475	5.1941			
PREM (10^{-3} Hz)	4.0323	4.4698	5.0744	4.3003	4.8453	5.1938			

large-scalar heterogeneity of the mantle. So ${}_{10}S_2$ mode is sensitive to the shear-wave parameter in the inner core, while ${}_{13}S_2$ mode is susceptible to the compressive-wave parameter in the top of the inner core. ${}_7S_{13}$ is a susceptible mode of the shear-wave parameter in the top of the inner core, however the amplitude of ${}_7S_{13}$ mode was often too low to observe. A kind of EFO modes like ${}_{10}S_2$, ${}_{13}S_2$ and ${}_7S_{13}$ were also called ‘inner core sensitive’ modes, which were usually applied to the investigation of the deep structure of the Earth.

The checked ${}_{12}S_1$ mode had a higher frequency than the theoretical prediction and it was sensitive to the shear-wave velocity of some layers in the mantle, which suggested that these layers might have a higher shear-wave velocity than PREM model^[24] in the mantle. It was difficult for us to judge whether the observed ${}_7S_{10}$ mode mainly mirrors the elastic parameters in the lower mantle or the upper mantle, because ${}_7S_{10}$ mode was a sensitive mode of the shear wave in the lower mantle and the compressive wave in the upper mantle. ${}_7S_{13}$ mode is hypersensitive to the shear-wave velocity in the

top of the inner core, which can provide us a valuable way to investigate the characteristics of the Earth’s deep structure. However it was very difficult for us to observe usually. The checked ${}_7S_{13}$ mode had a lower frequency than the prediction of PREM model and even much lower than that of CORE II model^[25], which suggested that the shear-wave velocity was clearly lower than the prediction of present models, in other words, the real rigidity might be lower than the present theoretical estimation in the top of the inner core.

3 Check of EFO spectral splitting and discussions

EFO modes produce the spectral splitting phenomena instead of the spectral degeneration^[26] because of the effect of the Earth’s rotation and ellipticity, at the same time, the spectral splitting phenomena of EFO modes are also created by the anisotropy of the inner core and the lateral heterogeneity in the mantle^[27,28]. So the splitting phenomena of EFO can provide a valuable way to in-

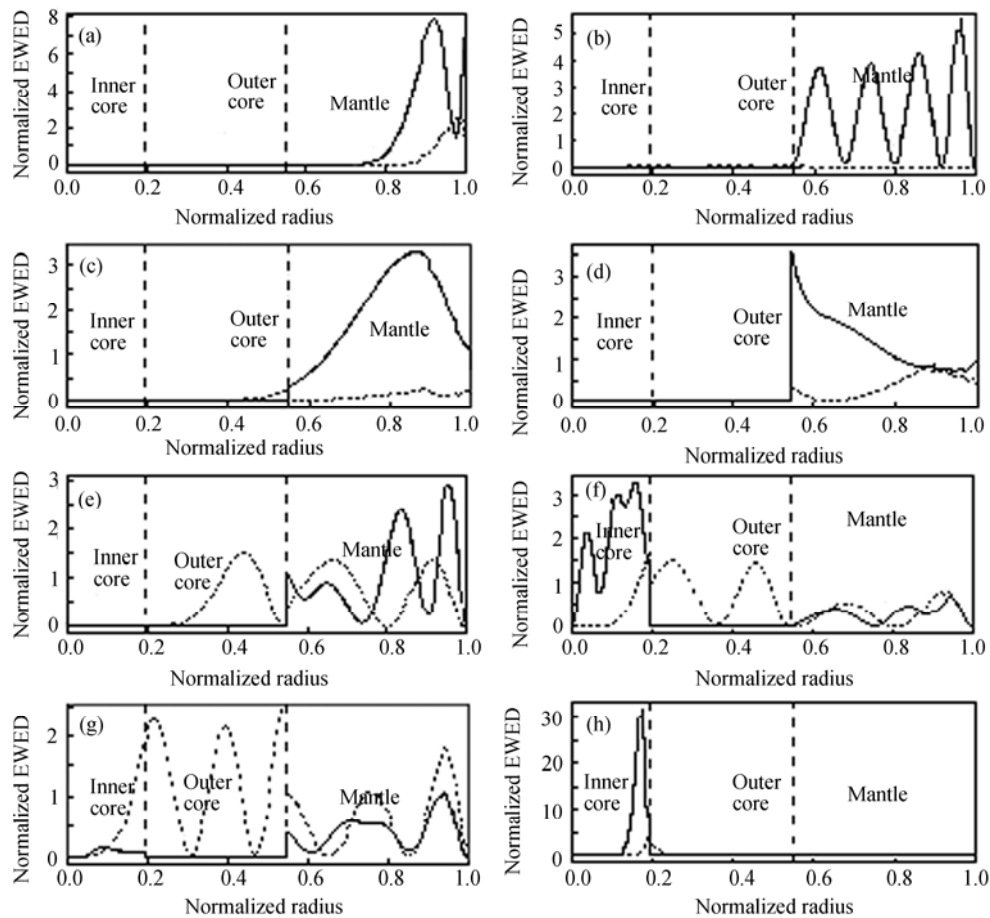


Figure 2 The kernel functions of some modes. Elastic-wave energy density is the function of radius in the Earth, and the energy has been normalized so that the total elastic-wave energy of a mode is unity. Shear-energy density (solid line) and compressive-energy density (dashed line) for selected spheroidal modes. Horizontal ordinate is the normalized radius (radius = 1 is surface), vertical ordinate is normalized elastic-wave energy density (abbrev: Normalized EWED). (a) ${}_0S_{24}$ mode; (b) ${}_{12}S_1$ mode; (c) ${}_1S_4$ mode; (d) ${}_0S_3$ mode; (e) ${}_8S_6$ mode; (f) ${}_{10}S_2$ mode; (g) ${}_{13}S_2$ mode; (h) ${}_7S_{13}$ mode.

investigate the deep inner structure of the Earth and its geodynamics mechanics^[29,30]. Woodhouse et al.^[31] introduced the splitting function of EFO modes to study the anisotropy of the Earth's inner core. Giardin et al.^[32], He and Tromp^[29] and Ishii et al.^[28] separately applied the abnormal splitting phenomena to the study of the Earth's deep construction. Laske & Masters^[33] discussed the anisotropy and the difference rotation of the inner core by analyzing the abnormal spectral splitting of EFO.

On the basis of the excellent theoretical work provided by Dahlen et al.^[26], the mature theory had been built to study the spectral splitting of EFO effected by the Earth's rotation and ellipticity, so we can compare the observed spectral splitting phenomena with the theoretical predictions of some Earth's models such as PREM model^[24]. Every splitting mode consists of two or more than two splitting peaks. The observed splitting

width of an EFO mode is the difference frequency between the highest-frequency peak and the lowest-frequency peak and it is marked as W_{ob} . The theoretical splitting width of an EFO mode can be calculated on the basis of PREM model with the effect of the Earth's rotation and ellipticity^[26, 32] and it is signed as W_{th} . For the convenience of splitting analysis, some researchers^[29,32] adopted a ratio value between the observed splitting width W_{ob} and the theoretical splitting width W_{th} as the splitting ratio, which was marked as R and used to evaluate the splitting phenomena of EFO modes usually.

The dW value is the difference frequency between the observed splitting width W_{ob} and the theoretical splitting width W_{th} , which describes the contribution of both the anisotropy of inner core and the lateral heterogeneity in the mantle to the spectral splitting of EFO^[29,32]. In general, dW was brightly smaller than W_{th} the effect of the Earth's rotation and ellipticity, so R values usually ap-

proached 1, this kind of EFO splitting phenomena was often called the normal spectral splitting of EFO modes^[4,10]. Masters et al.^[30] found that some EFO modes occupied the dW values close to their W_{th} values, even dW values of a few modes went beyond the W_{th} values. This meant that the R values of these modes were larger than 1.0 and even exceeded 2.0, and suggested that it was not neglected for some EFO modes to consider the effect of anisotropy of inner core and the lateral heterogeneity of the mantle. This kind of EFO splitting phenomena was usually called the abnormal spectral splitting of EFO modes. The former investigations^[28,29,32] showed that the abnormal splitting phenomena mainly focused on the inner core sensitive modes, and most of abnormal splitting phenomena could be explained by the cylindrical anisotropy of the inner core. The dW values of these sensitive modes had some kind of proportion relationship with the anisotropy strength of the inner core^[28], in other words, the R values were also proportional to the anisotropy strength of the inner core. So the larger the R values of sensitive modes are, the stronger anisotropy it means in the inner core. On the contrary, the weaker anisotropy it means in the inner core.

Many splitting EFO modes were excited by Sumatra-Andaman Large Earthquake, we have investigated the splitting phenomena of 12 EFO modes including ${}_0S_2$, ${}_0S_3$, ${}_1S_2$, ${}_1S_4$, ${}_1S_7$, ${}_2S_6$, ${}_3S_2$, ${}_5S_4$, ${}_5S_5$, ${}_{10}S_2$, ${}_{13}S_2$ and ${}_{13}S_3$ in this paper. The observation results of these modes are listed in Table 3, and the splitting peaks of 4 modes are shown in Figure 3. All peaks of these splitting modes possessed the SNR values of more than 3, which showed that it was reliable for the check of these splitting modes. Among those 12 splitting EFO modes, there were 9 modes (including ${}_0S_2$, ${}_0S_3$, ${}_1S_2$, ${}_1S_4$, ${}_1S_7$, ${}_2S_6$, ${}_3S_2$, ${}_5S_4$ and

${}_5S_5$ mode) with the R values approximately equal to 1, which were considered as the normal splitting mode. ${}_{10}S_2$, ${}_{13}S_2$ and ${}_{13}S_3$ modes were considered as the abnormal splitting modes, because their R values were clearly larger than 1.0 or even beyond 2.0^[30,31]. The splitting width of ${}_{10}S_2$ mode is susceptible of the shear wave in the top of the inner core, while the splitting width of ${}_{13}S_2$ mode is sensitive to the compressive wave in the top of the inner core as well as ${}_{13}S_3$ mode. So the larger the R values of sensitive modes were, the stronger anisotropy it meant in the inner core. Laske and Masters^[33] investigated the anisotropy of the inner core by analyzing the abnormal splitting of sensitive modes, and provided the important constraint of the difference rotation of the inner core. There have not been the former example for the observation of sensitive modes and their splitting in China so far, we first observed three sensitive modes and their spectral splitting excited by Sumatra-Andaman Large Earthquake in this paper.

Giardini et al.^[32] at the Harvard University investigated the splitting ratio R of some EFO modes with the observational data of long-period seismographs, which were very accurate and often referenced by the others, their R values were separately equal to 3.45, 2.40 and 1.74 for ${}_{10}S_2$, ${}_{13}S_2$ and ${}_{13}S_3$ modes. Our observed R values were respectively equivalent to 1.98, 3.72 and 2.32 for the three modes. There is a clear difference between our observational results and the former results^[32] for ${}_{10}S_2$ mode, our checked R value (1.98) was brightly less than the former observation (3.45), it meant that the shear-wave anisotropy in the inner core might be lower than the former estimation provided by Giardini et al.^[32], which was basically consistent with our result discussed in the former chapter that the rigidity in the inner core might be lower than the theoretical prediction of PREM.

Table 3 Spectral splitting of 12 EFO modes checked by superconducting gravimeter C0-32 at wuhan station

Modes	${}_0S_2$	${}_0S_3$	${}_1S_2$	${}_1S_4$	${}_1S_7$	${}_2S_6$	${}_3S_2$	${}_5S_4$	${}_5S_5$	${}_{10}S_2$	${}_{13}S_2$	${}_{13}S_3$
Lowest-frequency (10 ⁻³ Hz)	0.2996	0.4605	0.6759	1.1611	1.6484	1.6786	1.0992	2.3742	2.7110	4.0354	4.8376	5.1892
SNR	66.3	166.2	6.0	38.0	102.0	11.0	45.5	11.2	13.27	3.6	7.9	12.0
Highest-frequency (10 ⁻³ Hz)	0.3194	0.4753	0.6858	1.1809	1.6612	1.6860	1.1067	2.3817	2.7085	4.0429	4.8624	5.2015
SNR	60.1	313.3	10.5	368.2	91.9	27.4	46.5	8.3	22.44	12.5	6.3	7.2
W_{ob} (10 ⁻⁶ Hz)	19.8	14.8	9.9	19.8	12.8	7.4	7.5	7.5	7.5	7.5	24.8	17.3
W_{th} (10 ⁻⁶ Hz)	19.48	13.05	11.43	18.33	13.15	7.28	6.49	6.82	8.24	3.79	6.66	7.47
dW (10 ⁻⁶ Hz)	0.32	1.75	-1.53	1.47	-0.35	0.12	1.01	0.68	-0.74	3.71	18.14	9.83
R	1.07	1.13	0.87	1.08	0.97	1.02	1.16	1.10	0.91	1.98	3.72	2.32

W_{ob} is the observed splitting width of an EFO mode, W_{th} is the theoretical splitting width of an EFO mode with the effect of Earth's rotation and ellipticity based on PREM model^[26,32], $dW = W_{ob} - W_{th}$; splitting ratio of an EFO mode is described as $R = W_{ob}/W_{th}$.

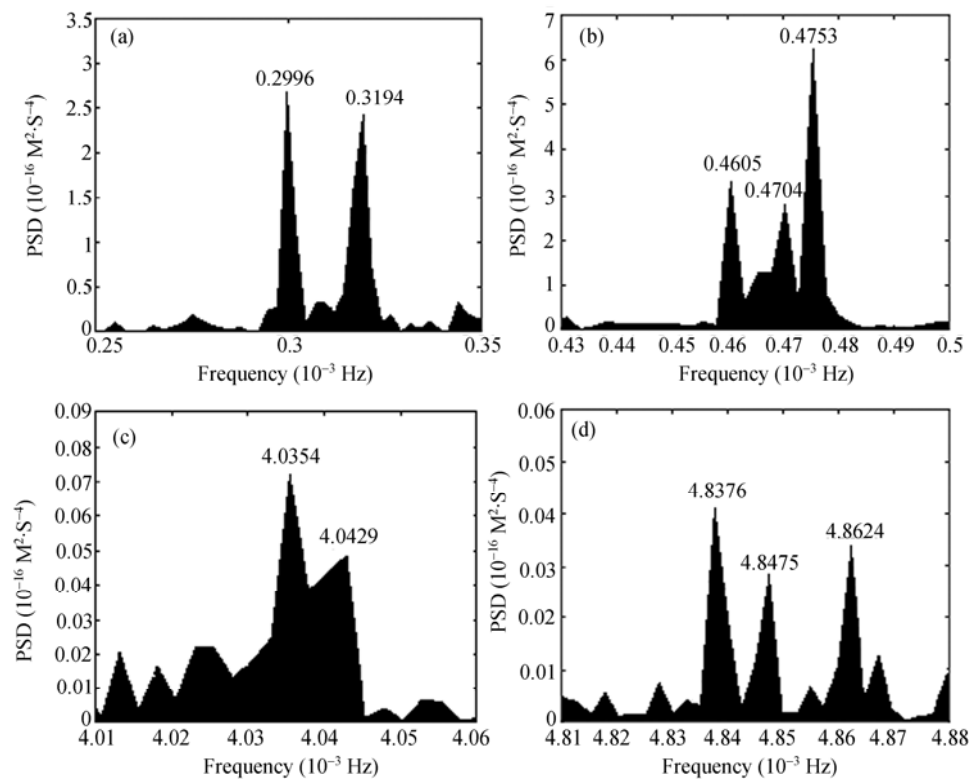


Figure 3 Splitting peaks of some EFO modes checked by SG C0-32. Horizontal ordinate is frequency, vertical ordinate is power spectral density. (a) 0S_2 mode; (b) 0S_3 mode; (c) ${}_{10}S_2$ mode; (d) ${}_{13}S_2$ mode.

However, our observed R values (3.72 and 2.32) were separately much larger than the former observation values (2.40 and 1.74)^[32] for ${}_{13}S_2$ and ${}_{13}S_3$ modes, which manifested that the compressive-wave anisotropy in the top of the inner core was not only very strong but also brightly higher than the former estimations. At present the researchers^[30–34] generally believed that the anisotropy of the inner core was originated from its rotation and presented a kind of cylindrical anisotropy. The shear-wave anisotropy should be in agreement with the compressive-wave anisotropy for the cylindrical inner core, so there was a noticeable contradiction between the observed shear-wave anisotropy and the checked compressive-wave anisotropy in the top of the inner core. This suggested that the anisotropy of the inner core could be much more complicated than what is known to us at present, and there might be some new geodynamic mechanics during the formation of the inner core.

4 Conclusions and discussions

4.1 Check of fundamental and harmonic EFO modes

The accident of Sumatra-Andaman Large Earthquake was accurately recorded by the superconducting gra-

vimeter C0-32 at Wuhan station. After the process and analysis on the observation data of SG C0-32, we caught in total 93 EFO modes consisting of 42 fundamental modes, 2 radial modes and 49 harmonic modes. It was the first time that the harmonic mode series were systematically observed by SG, which provided the fundamental observation results for the investigation of the deep inner structure of the Earth.

4.2 Check of EFO splitting phenomena and discussions on the anisotropy of the inner core

By analyzing the splitting phenomena of EFO modes excited by Sumatra-Andaman Large Earthquake, we clearly caught the spectral splitting of 12 modes, especially the abnormal spectral splitting of ${}_{10}S_2$, ${}_{13}S_2$ and ${}_{13}S_3$. On the basis of the discussions of some sensitive modes and abnormal splitting phenomena, we considered that the observed shear-wave anisotropy in the inner core was lower than the former estimation^[32], however the compressive-wave anisotropy in the inner core was higher than the former estimation^[32]. This implied that the anisotropy of the inner core was very complicated, and there might be some new geophysical phenomena in the formation process of the inner core.

The observation data of SG C0-32 were provided by Prof. Hao Xinhua in the geodynamic observation station of the Jiufeng Mountain under Institute of Geodesy and Geophysics, Chinese Academy of Sciences. MINOS program

(FORTRAN) was mostly written by Freeman Gilbert and Guy Masters, IGPP, UCSD, La Jolla, California, and Dr. Widmer-Schmidrig made a web version of MINOS program. We expressed our sincere thanks for their help.

- 1 Stein S, Okal E A. Speed and size of the Sumatra earthquake. *Nature*, 2005, 434 (7033): 581—582
- 2 Park J, Song TRA, Tromp J, et al. Earth's free oscillations excited by the 26 December 2004 Sumatra-Andaman earthquake. *Science*, 2005, 308 (5725): 1139—1144
- 3 Crossley D J, Hinderer J. Global Geodynamics Project — GGP: status report 1994. In: Poitevin C, ed. *Proceeding of the Workshop on Non-tidal Gravity Changes*. via Conseil de L'Europe Cahiers du Centre Européen de Géodynamique et de Séismologie, Lux-embourg, 1995, 11: 244—269
- 4 Rosat S, Hinderer J, Crossley D, et al. Performance of superconducting gravimeters from long-period seismology to tides. *J Geodyn*, 2004, 38(3-5): 461—476
- 5 Rosat S, Sato T, Imanishi Y, et al. High-resolution analysis of the gravest seismic normal modes after the 2004 Mw=9 Sumatra earthquake using superconducting gravimeter data. *Geophys Res Lett*, 2005, 32 (13): Art. No. L13304
- 6 Sun H P, Chen X D, Xu H Z, et al. the accurate determination of tidal observation factors of GWR superconducting gravimeter. *Acta Seismol Sin (in Chinese)*, 2001, 23(6): 651—658
- 7 Xi Q W. The computation for theoretical values of earth tides. *Acta Geophys Sin (in Chinese)*, 1982, 25(suppl.): 632—643
- 8 Tamura Y. A Harmonic Development of the tide-Generating Potential. *Bull D'infor. Marees Terrestres.*, 1987, 101: 6813—6824
- 9 Xu H Z, Sun H P, Xu J Q, et al. International tidal gravity reference values at Wuhan station: *Sci China Ser D-Earth Sci*, 2000, 43(1): 77—83
- 10 Ness N R, Harrison C T, Slichter L B. Observation of the free oscillation of the earth. *J Geophys Res*, 1961, 66(2), 621—629.
- 11 Van Camp M. Measuring Seismic normal modes with the GWR C021 Superconducting gravimeter. *Phys Earth and Plan Int*, 1999, 116: 81—92
- 12 Neumeier J, Bathelmes F, Combrinck L, et al. Analysis results from the SG registration with the dual sphere superconducting gravimeter at SAGOS (South Africa). *Bull D'infor Marees Terrestres*, 2002, 135: 10607—10616
- 13 Lei X E, Xu H Z, Sun H P. Check of free oscillation signal with SG data, *Chin Sci Bull*, 2002, 47(8): 1573—1578
- 14 Lei X E. the Study and check of the FCN parameters and the earth's free oscillations. Thesis for Doctor Degree (in Chinese), Beijing: Graduate Univ Chin Acad Sci, 2003, 170
- 15 Niebauer T M. Correcting gravity measurements for the effects of local air pressure. *J Geophys Res*, 1988, 93(B7): 7989—7991
- 16 Farrell W E. Deformation of the earth by the surface loads. *Rev Geophys Space Phys*, 1972(10): 761—797
- 17 Merriam J B. Atmospheric pressure and gravity. *Geophys J Ints*, 1992(109): 488—500
- 18 Sun H P. Atmospheric pressure and gravity. *Chin Sci Bull*, 1997, 42(1), 1712—1719
- 19 Xu J Q, Hao X H, Sun H P. Influence of atmospheric pressure on tidal gravity at Wuhan station. *Acta Geophys Sin (in Chinese)*, 1999, 28(1): 21—27
- 20 Luo S C. Study on the loading effects of the atmospheric pressure. Thesis for Doctor Degree (in Chinese), Beijing: Grad Univ Chin Acad Sci, 2003, 141
- 21 Zürn W, Widmer R. On noise reduction in vertical Seismic records below 2 mHz using local barometric pressure. *Geophys Res Lett*, 1995(22): 3537—3540
- 22 Banka D, Jentzsch G, Crossley D. Investigations of superconducting gravimeter records in the frequency range of the free oscillations of the Earth — the noise magnitude. *Proc.13th Symp. Earth Tides*, Brussels, 1998, 641—648
- 23 Lei X E, Xu H Z, Sun H P. Detection of spheroidal free oscillation excited by Peru 8.2 Ms earthquake with five international superconducting gravimeter data. *Sci China Ser D-Earth Sci*, 2005, 48(1): 123—133
- 24 Dziewonski A, Anderson D. Preliminary reference earth model. *Phys Earth Planet Int*, 1981, (25): 297—356
- 25 Widmer R, Masters G, Gilbert F. Spherically symmetric attenuation within the earth from normal mode data. *Geophys J Int*, 1991, 104: 541—553
- 26 Dahlen F A. The normal modes of a rotating, elliptical earth. *Geophys J R Astr*, 1968(16): 329—367
- 27 Ishii M, Tromp J. Normal-mode and free-air gravity constraints on lateral variations in velocity and density of Earth's mantle. *Science*, 1999, 285(5431): 1231—1236
- 28 Ishii M, Tromp J, Dziewonski A M, et al. Joint inversion of normal mode and body wave data for inner core anisotropy: Laterally homogeneous anisotropy. *J Geophys Res*, 2002, 107(B12): 2379—2395
- 29 He X, Tromp J. Normal-mode constraints on the structure of the Earth. *J Geophys Res*, 1996, 110(B9): 20053—20082
- 30 Masters G, Gilbert F. Structure of the inner core inferred from observations of its spheroidal shear modes. *Geophys Res Lett*, 1981(8): 569—571
- 31 Woodhouse J H, Giardini D, Li X D. Evidence for inner core anisotropy from free oscillations. *Geophys Res Lett*, 1986(13): 1549—1552
- 32 Giardini D, Li X D, Woodhouse J H. Splitting Functions of Long-Period Normal Modes of the Earth. *J Geophys Res*, 1988(93): 13716—13742
- 33 Laske G, Masters G. Limits on differential rotation of the inner core from an analysis of the Earth's free oscillations. *Nature*, 1999, 402 (6757): 66—69
- 34 Tromp J. Inner-core anisotropy and rotation. *Ann Rev Earth Planet Sci*, 2001, 29: 46—69